

MemANNS: Enhancing Billion-Scale ANNS Efficiency with Practical PIM Hardware

Sitian Chen¹, Amelie Chi Zhou¹, Yucheng Shi¹, Yusen Li², Xin Yao³

¹Hong Kong Baptist University ²Nankai University ³Huawei

Abstract

In numerous production environments, including information retrieval and recommendation systems, Approximate Nearest Neighbor Search (ANNS) plays an indispensable role, particularly when dealing with massive datasets that can contain billions of entries. The necessity for rapid response times in these applications makes the efficiency of ANNS algorithms crucial. However, traditional ANNS approaches encounter substantial challenges at the billion-scale level. CPU-based methods are hindered by the limitations of memory bandwidth, while GPU-based methods struggle with memory capacity and resource utilization efficiency.

This paper introduces *MemANNS*, an innovative framework that utilizes UPMEM’s Processing-in-Memory (PIM) architecture to address the memory bottlenecks in ANNS algorithms at scale. We concentrate on optimizing a well-known ANNS algorithm, IVFPQ, for PIM hardware through several techniques. First, we introduce an architecture-aware strategy for data placement and query scheduling that ensures an even distribution of workload across PIM chips, thereby maximizing the use of aggregated memory bandwidth. Additionally, we have developed an efficient thread scheduling mechanism that capitalizes on PIM’s multi-threading capabilities and enhances memory management to boost cache efficiency. Moreover, we have recognized that real-world datasets often feature vectors with frequently co-occurring items. To address this, we propose a novel encoding method for IVFPQ that minimizes memory accesses during query processing.

Our comprehensive evaluation using actual PIM hardware and real-world datasets at the billion-scale, show that MemANNS offers a significant 4.3x increase in Queries Per Second (QPS) over CPU-based Faiss, and it matches the performance of GPU-based Faiss implementations. Additionally, MemANNS improves energy efficiency, with a 2.3x enhancement in QPS/Watt compared to GPU solutions. These findings suggest that MemANNS can achieve superior performance within a comparable power envelope, highlighting its suitability for large-scale applications such as serving large models.

1 Introduction

Approximate Nearest Neighbor Search (ANNS) is widely used in many production systems, including data mining [43], information retrieval [33, 51], and recommendation systems [12, 36, 45]. In these systems, the data typically reaches into the

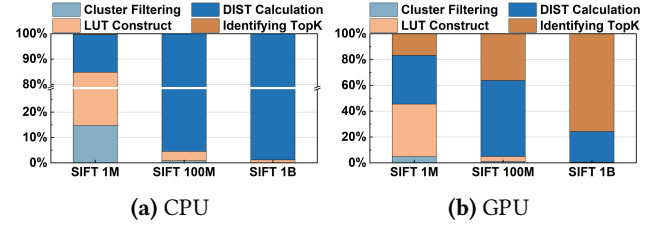


Figure 1. Query processing time breakdown of the IVFPQ [26] algorithm, using SIFT dataset [27] at different scales (1M, 100M and 1B). Hardware spec. see Section 5.

billions. For example, modern social network platforms serve billions of daily active users and provide real-time recommendations [50]. Further, these systems frequently operate under stringent latency constraints (e.g., real-time recommendations and interactive user serving), which underscores the critical importance of efficient ANNS algorithms.

ANNS algorithms are broadly classified into four main categories: hash-based [6, 20, 54], tree-based [8, 11, 53], graph-based [32, 40, 46] and compression-based [28, 30, 38]. While graph-based, tree-based and hash-based methods excel in handling million-scale searches, they encounter scalability challenges for billion-scale datasets due to their substantial memory demands. For example, HNSW [39], a graph-based method, consumes between 60-450 bytes of memory per vertex, resulting in up to 450GB data size for a graph with one billion vertices. In contrast, compression-based methods enable the encoding of extensive datasets into smaller storage footprints, which greatly enhances scalability and cost-efficiency. This is particularly beneficial for applications such as personalized recommendation and large model serving, where managing vast amounts of data is paramount. Thus, in this paper, we focus mainly on compression-based ANNS algorithms. Specifically, we focus on IVFPQ [26], a popular compression-based algorithm known for its effectiveness in reducing the storage of datasets while maintaining a high level of search accuracy.

IVFPQ answers nearest neighbor queries using four stages, namely cluster filtering, lookup table (LUT) construction, distance calculation and top-k identification (see Section 2.1 for details). We study the performance bottleneck of existing IVFPQ implementations [15] (CPU-based and GPU-based) and present their runtime breakdown in Figure 1. We adopt datasets with different sizes, from 1 million to 1 billion. We have two interesting observations. *First*, when data scales to billions, the performance bottleneck shifts significantly compared to smaller datasets. For example, when data scales

from 1 million to 1 billion, the performance bottleneck of the CPU-based implementation shifts from the LUT construction stage, which is mainly compute-intensive, to the distance calculation stage, which is mainly memory-bound. This is because the growing data size results in increased memory accesses to the encoded points, hence longer memory access time. *Second*, traditional IVFPQ implementations are facing different performance bottlenecks: at the billion scales, the CPU-based implementation is bounded by memory, while the GPU-based implementation is bounded by the top-k identification stage. This stage has limited parallelism, preventing full utilization of GPU resources and causing prolonged execution time.

The above observations reveal the limitations of existing ANNS solutions. *First*, due to the shifted performance bound at different scales, existing performance optimizations for million-scale ANNS [5, 28] may not be suitable to billion-scale. *Second*, traditional architectures have distinct limitations that result in performance bottlenecks in ANNS algorithms. That is, the CPU-based solutions suffer from low memory bandwidth, leading to memory bottlenecks, while the GPU-based solutions face low resource utilization, resulting in suboptimal performance and cost-efficiency. In this paper, we propose to adopt a new hardware architecture, namely the UPMEM Processing-in-Memory (PIM) hardware [2], to address the limitations of existing solutions.

UPMEM PIM is a standard DIMM device that integrates processing cores directly into memory chips, enabling in-memory computation to reduce data movement and enhance efficiency [14]. It features multi-threaded DPU cores with direct access to memory, significantly improving performance for data-intensive applications. While recent studies have explored the use of PIM/near-memory technology for ANNS, they are either designed for million-scale [47] or rely on simulated architectures [34, 37]. *To the best of our knowledge, this is the first study to leverage practical PIM hardware to enhance billion-scale ANNS performance.*

To fully utilize the computation and bandwidth resources provided by the UPMEM hardware, we face the following challenges. *First*, UPMEM PIM shows a high aggregated memory bandwidth, relying on the fact that the workload is balanced across all chips on the PIM hardware. However, achieving workload balance is difficult due to the diversity in data sizes and access frequencies of real-world datasets. *Second*, UPMEM’s unique hardware architecture requires a careful redesign of the ANN search process and efficient memory management strategy to leverage the full potential of PIM computing power and memory bandwidth. *Third*, although PIM has shown potential for accelerating memory-intensive applications [13], its hardware resources remain relatively limited compared to traditional CPUs and GPUs. This necessitates the design of pruning methods to reduce the workloads for PIM while preserving query accuracy.

In this paper, we propose *MemANNS*, an efficient framework for ANNS algorithms using UPMEM PIM hardware. *MemANNS* incorporates several techniques to address the above mentioned challenges individually. *First*, we introduce an architecture-aware data placement and query scheduling approach to achieve workload balance and maximize the aggregated memory bandwidth of available PIM chips (Section 4.1). *Second*, we design an efficient thread scheduling approach to fully utilize the multi-threaded computing power on PIM, together with efficient memory management to maximize cache reuse on PIM to further improve the performance (Section 4.2). *Third*, on observing the fact that in real-world datasets, there are often some items that appear together in data point vectors [49]. We propose to redesign the encoding in IVFPQ and pre-store the frequently accessed item combinations at offline to reduce the memory accesses at online phase, hence reducing query answering time (Section 4.3). *Lastly*, we optimize the top-k identification stage with thread-local top-k heap and early pruning to reduce the selection time (Section 4.4). Note that although most of our discussions surround IVFPQ, the framework can also be applied to other quantization-based ANNS algorithms.

We evaluated the performance of *MemANNS* using 7 UPMEM PIM modules and real-world billion-scale datasets. Experiments have shown that, *MemANNS* can improve the Query per Second (QPS) by 4.3x compared to Faiss [15] on CPU, and is comparable to GPU-based Faiss implementation. When comparing the cost-effectiveness, *MemANNS* improves the QPS/Watt by 2.3x compared to GPU-based Faiss. That means, if given the same power budget, *MemANNS* can achieve much better performance than GPU-based ANNS solution. In addition, *MemANNS* demonstrates near-linear scalability for large-scale datasets, which makes it a promising solution for practical applications such as large model serving [37].

2 Background and Motivation

2.1 Approximate Nearest Neighbor Search (ANNS)

ANNS algorithms are commonly employed to identify the top-k most similar vectors to a query vector within a given set of vectors. Among the various ANNS algorithms available, our study focuses on the Inverted File with Product Quantization (IVFPQ) method [26], which is one of the most popular algorithms for ANNS due to its efficiency in managing large-scale datasets. Figure 2 illustrates a simple example of the IVFPQ process, which can be divided into two phases, namely the *offline* phase (top) and *online* phase (bottom).

Offline Phase: The offline phase of the IVFPQ algorithm prepares a dataset for efficient search by creating a compact representation. It employs two key techniques: Inverted File (IVF) and Product Quantization (PQ). IVF clusters search points into $|C|$ clusters using methods like K-means and computes residuals, which are the differences between each point

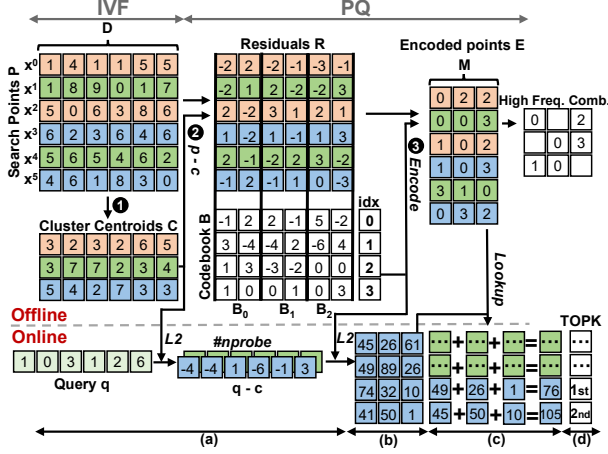


Figure 2. An example of the IVFPQ algorithm (L2 distance).

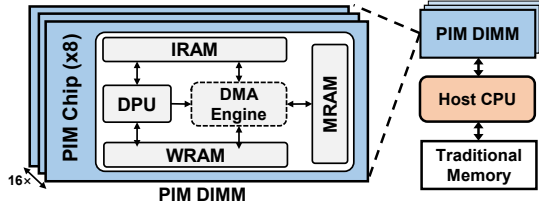


Figure 3. UPMEM PIM architecture.

and its cluster centroid. PQ then compresses these residuals by dividing vectors into M subvectors and encoding them using a codebook B . Each encoded point in E is an identifier that maps to a specific codeword in the codebook. Practical implementations often use *uint8* encoding of an identifier, achieving a compression rate of $4D/M$. This preprocessing enables faster query searches in the online phase.

Online Phase: When a query vector q arrives, the online phase initiates a four-stage process to find the k nearest vectors to q . (a) *Cluster Filtering*: The distances between q and each centroid vector c stored in IVF are calculated and the $nprobe$ s closest centroids are selected for further processing. (b) *Look-up Table (LUT) Construction*: For each selected centroid, an LUT is created to store pre-computed information and eliminate redundant calculations during query searching. Specifically, each element $LUT[j][i]$ represent the distance between the j -th vector of sub-codebook B_i and the i -th sub-segment of the $q - c$ vector. To get the distance from q to a search point x , we can look up and accumulate the values in LUTs as: $L2(q, x) = L2(q - c, r) = \sum_{i=0}^{M-1} LUT[e_i][i]$, where r and e are the residual and encoded vectors of x , respectively. (c) *Distance Calculation*: Using the LUTs, distances from q to all points in the selected clusters are computed by looking up and aggregating the partial distances stored in the LUTs. (d) *Identifying Top-K*: Lastly, all computed distances are sorted, and the k vectors with the shortest distances are identified as the approximate nearest neighbors.

2.2 UPMEM PIM Architecture

Processing-in-Memory (PIM) represents a promising paradigm for addressing the data movement bottleneck encountered in many large-scale data analytics applications including ANNS. Recently, real PIM hardware has started to enter the market, with UPMEM PIM being the first commercially available solution [2, 14]. It has been applied in recommendation systems [13], graph processing [10, 18], machine learning [19, 42] and database systems [9, 29] to mitigate the memory wall issue. The potential of UPMEM PIM for ANNS algorithms has never been explored.

Figure 3 shows the structure of a UPMEM module, which is a standard DDR4 DIMM module that integrates 16 PIM chips. Each chip encompasses 8 processing cores, referred to as DRAM Processing Units (DPUs). Each DPU is a multi-threaded 32-bit RISC core with a specific ISA [3]. This core supports up to 24 hardware threads running at 350 MHz, featuring a 14-stage pipeline. Each DPU has exclusive access to a 64MB DRAM bank named MRAM, a 24KB instruction memory IRAM, and a 64KB scratchpad memory WRAM. DPUs leverage WRAM for processing tasks, and each WRAM access is finished in a single cycle. DPUs have no direct access to MRAM. MRAM accesses are mediated by a DMA engine, with a latency far greater than that of WRAM accesses [22].

The host CPU interacts with MRAM for data transfer and retrieval. Data transfers between the host CPU and DPUs can happen concurrently if the buffer sizes transferred to/from all MRAM banks are the same; otherwise, the transfers occur sequentially. Notably, inter-DPU communication relies on the host CPU [23]. Existing UPMEM PIM systems can support up to 20 DIMMs, each housing 16 chips, enabling a maximum of 2560 DPUs working simultaneously. Given that each DPU has a private connection to its local MRAM, this provides a significant data access bandwidth of up to 7.2 TB/s [10], significantly surpassing the memory bandwidth typically available to CPUs.

2.3 Motivation and Challenges

In this subsection, we discuss the opportunities and challenges associated with PIM-based ANNS acceleration.

Opportunities. As shown in Figure 1, traditional computing architectures encounter various performance bottlenecks as data sizes scale to billions in ANNS algorithms. Specifically, for a dataset with one billion vectors, the distance calculation stage, which involves multiple rounds of LUT lookups to retrieve partial distances, requires a total number of $\frac{10^9}{|C|} \times nprobe \times M$ memory accesses. For the example in Figure 1, we set M and $nprobe$ to 32 and $|C|$ to 4096, resulting in 250 million random memory accesses per query. This shows significant challenges related to memory bandwidth and latency when deployed on conventional systems. The high aggregated memory bandwidth of the UPMEM PIM architecture (i.e., up to 7.2 TB/s [10]) provides an excellent

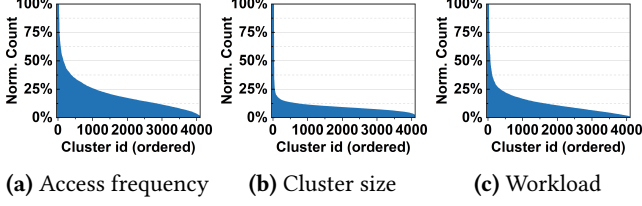


Figure 4. The distribution of access frequency, cluster size and workload in each cluster in SPACEV1B [1].

opportunity to mitigate the memory bottleneck and enhance the overall efficiency of ANNS implementations. Although GPUs also provide high memory bandwidth, they often suffer from limited memory capacity. In contrast, the UPMEM PIM offers a scalable solution for managing larger data sizes, thanks to its standard DIMM form factor.

Challenges. The advantage of UPMEM PIM for ANNS stems from its high *aggregated* memory bandwidth. However, individual DPUs possess restricted storage capacity, computational power, and memory bandwidth. Fully utilizing these resources to create an efficient PIM-based ANNS solution is not easy, particularly with the imbalanced data access pattern and complicated PIM resource management.

Challenge 1: Imbalanced data access pattern. As illustrated in Figure 3, each PIM DIMM consists of 128 DPUs, each with fast and exclusive access to its local memory (i.e., WRAM, IRAM and MRAM). Data communications between DPUs have to go through the host CPU, which is much slower than intra-DPU data access. Thus, it is crucial to have optimized data distribution across DPUs to 1) avoid inter-DPU/CPU-DPU communications as much as possible, and 2) achieve balanced memory accesses across DPUs to maximize the aggregated memory bandwidth. However, achieving this goal is non-trivial, mainly due to the imbalanced data distribution in *cluster popularity* and *cluster size*.

We analyzed the access frequencies of different clusters in IVFPQ using the SPACEV1B dataset and found that certain clusters are accessed much more frequently than others (up to 500x) as shown in Figure 4a. Further, Figure 4b illustrates that some clusters contain significantly higher numbers of data points (up to 10^6 x). As a result, the two factors lead to much skewed workload across clusters, making it challenging to achieve workload balance across DPUs.

Challenge 2: Complicated PIM resource management. The UPMEM architecture provides parallel structure between DPUs. Each DPU equips with up to 24 hardware threads and a 14-stage pipeline, with exclusive access to its local memory. How to adapt the IVFPQ method to fully utilize the multi-threads and leverage the 14-stage pipeline to maximally reduce the pipeline bubble and hide the memory read latency is a challenging problem. In addition, the fast WRAM on DPU has a limited capacity of 64KB only. Due to the significant bandwidth difference between WRAM and MRAM, we

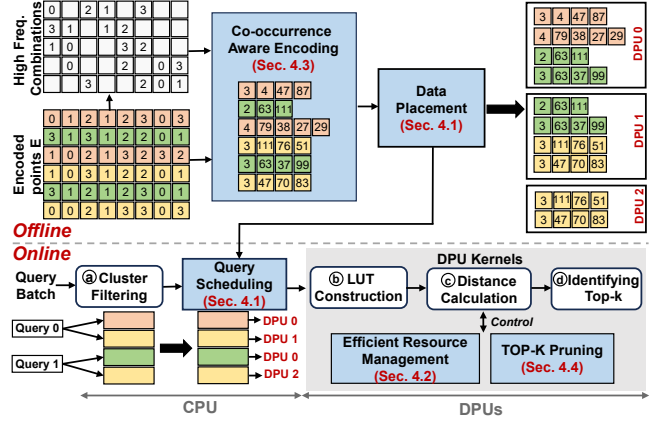


Figure 5. Overview of MemANNS. The key optimizations are highlighted in blue.

should maximize the amount of data stored in WRAM to improve performance. However, UPMEM lacks a Memory Management Unit (MMU) to virtualize its physical memory. DPUs use physical addresses when accessing memory [23], which prohibits efficient utilization of the limited cache space.

Challenge 3: Limited power of UPMEM PIM. Although UPMEM PIM is equipped with plentiful DPUs (128 per DIMM) and multiple memory layers, its power remains limited in comparison to CPUs with large cores and GPUs boasting thousands of cores. While PIM’s in-memory processing can significantly reduce data movement and associated latencies, the amount of data that can be efficiently processed by these DPUs are constrained. This limitation becomes more pronounced when apply PIM to billion-scale ANNS. This necessitates the design of pruning methods to reduce the workloads for PIM while preserving query accuracy.

In the following section, we give an overview of our MemANNS framework and briefly introduce the techniques proposed in response to these challenges.

3 System Overview

In viewing the limitations of existing ANNS solutions, this paper presents MemANNS, an efficient system that accelerates the ANN search using UPMEM PIM hardware. Figure 5 shows an overview of our system. The offline phase is executed on the host CPU to prepare and transfer data to DPUs for online processing. The cluster filtering stage of the online phase is executed on the host CPU to filter clusters and the rest stages are executed on the DPUs to utilize their high aggregated memory bandwidth. Optimizations have been proposed to improve the efficiency and performance of the offline and online phases of the IVFPQ algorithm separately.

Offline Optimizations. Recall that the offline phase uses IVF and PQ techniques to encode data points into smaller sizes. The encoded data are subsequently transferred to PIM for further processing. We propose two techniques for the offline phase. First, we propose a *PIM-aware data placement*

technique which strategically distributes encoded vectors across hundreds of DPUs, ensuring a balanced workload for optimized performance (tackling Challenge 1). Second, we design a *co-occurrence aware vector encoding* strategy that takes item co-occurrences into account to reduce the memory accesses during online search, thereby alleviating the workload pressure on PIM (tackling Challenge 3).

Online Optimizations. The online phase of IVFPQ takes a batch of queries as input, and conducts four stages to search for the nearest neighbors in the encoded vectors for the query vectors. We accelerate the online search process by deploying the most memory-intensive stages onto PIM to utilize its high aggregated memory bandwidth. We mainly propose the following optimizations to fully utilize PIM resources. First, we propose a balanced *query scheduling* approach to map the search workloads onto different DPUs, considering the placement of encoded vectors decided at offline phase. This scheduling approach works together with the data placement to achieve workload balance. Second, we propose two PIM *resource management* techniques, including thread scheduling and memory management, to fully explore the capabilities of PIM (tackling Challenge 2). Third, to prevent the top-k identification stage becoming a new bottleneck in PIM, as illustrated in Figure 1 for GPUs, we propose a top-k pruning technique to improve its performance.

4 Technical Details

This section presents the technical details of the optimization techniques in MemANNS, and explains how they tackle the challenges mentioned in Section 2.3.

4.1 PIM-Aware Workload Distribution

The workload distribution task includes two sub-tasks, namely the *data placement at offline time* and *query scheduling at online phase*. The data placement task tries to distribute the encoded data points across DPUs as balanced as possible, considering the variant cluster access frequencies and cluster sizes; while the query scheduling task tries to map the filtered clusters of all queries in the batch to different DPUs to actually balance the workload at runtime.

Offline Data Placement. The goal of the data placement is two-fold, namely avoiding inter-DPU/CPU-DPU data transfers and balancing the online data searching workload (i.e., the amount of memory accesses to the MRAM).

Considering that the online phase processes data according to clusters, a natural idea is to place an entire cluster in the same DPU, and maintain a local top-k list on each DPU for a query. The local top-k are then transferred to the CPU to generate the final top-k. By placing an entire cluster in a single DPU, we reduce the amount of partial top-k transmitted for a query, alleviating the communication bottleneck between DPUs and the host CPU. Following this

Algorithm 1 Data Placement for Cluster i

Input: $ndpu$: the number of available DPUs; s_i : #vectors in cluster i ;
 f_i : the access frequency of cluster i ; \bar{W} : the average workload per DPU;
 MAX_DPU_SIZE : the maximum number of vectors each DPU can have;
Output: dpu_id ;
1: $d_id \leftarrow ndpu, thld \leftarrow 1.0$ and $rate \leftarrow 0.02$;
2: $ncpy = \lceil s_i * f_i / \bar{W} \rceil$; $\triangleright ncpy$ denotes #DPUs that cluster i is distributed onto;
3: $w_i = s_i * f_i / ncpy$; $\triangleright w_i$ denotes the per DPU workload of cluster i ;
4: **while** $ncpy > 0$ **do**
5: **if** $W[d_id] + w_i \leq \bar{W} * thld$ **and** $S[d_id] + s_i \leq MAX_DPU_SIZE$ **then**
6: $dpu_id.push(d_id), ncpy \leftarrow ncpy - 1$;
7: $d_id \leftarrow (d_id + 1) \bmod ndpu$;
8: **if** $d_id == ndpu$ **then** \triangleright no suitable DPU found;
9: $thld \leftarrow thld + rate$; \triangleright enlarge threshold to loosen the workload balance constraint;

idea, we make data placement decisions based on clusters. Algorithm 1 shows the flow of our data placement approach.

The workload of a cluster is mainly contributed by the memory-intensive distance calculation stage, which performs excessive memory search in LUTs to calculate distances between a query q and all search points in the cluster. Thus, we can estimate the workload of a cluster i as follows. Let s_i denote the size of cluster i and f_i denote the frequency with which cluster i is used to process queries. The workload of cluster i can be represented as $w_i = s_i * f_i$. Given n DPUs and a batch of queries, the balanced memory accesses per DPU that we need to achieve is $\bar{W} = \frac{1}{n} \sum_i s_i \times f_i$, where f_i is derived from a predictor based on historical query data. The basic idea of achieving workload balance is to distribute data clusters across DPUs so that the workload on each DPU approximates \bar{W} as closely as possible.

Due to the skewness in cluster popularity and size, some clusters may have workloads significantly exceeding \bar{W} . Thus, we create $ncpy$ copies of these high-demand clusters (Line 2) and distribute them across different DPUs. When such clusters are required, we schedule the queries to different copies to balance the workload. When placing each copy (ordered according to workload from high to low), we iterate over all DPUs with sufficient capacity and select the one that does not exceed \bar{W} after the cluster is placed (Line 5). If no suitable DPU is found, we relax the workload balance constraint by adjusting the parameter $thld$ (Line 9) and restart the search. At the end of this algorithm, each cluster is placed on a specific DPU (or a list of $ncpy$ DPUs).

Algorithm 1 optimizes the placement for one cluster, while it is also important to consider the cluster co-location problem according to their distances. We observe from real-world datasets that, clusters selected for a query are typically situated in close proximity. For example, as shown in Figure 6, the three centroids in the red circle are likely to be selected concurrently for the query. Note that, each cluster will generate a partial top-k, which will be transmitted to the CPU to generate the final top-k. As CPU-DPU communications go through the memory bus, which is much slower than intra-DPU data exchange, we need to reduce the amount of partial top-k generated during query processing. Thus, when a DPU

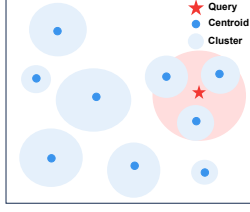


Figure 6. Inter-cluster Dis-

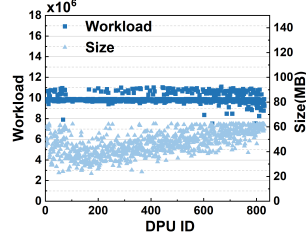


Figure 7. Workload distribu-

is selected for cluster i , we will continue to assign nearby clusters to the same DPU, based on inter-cluster distances, until the workload of the DPU reaches W . This will allow the partial top-k results of co-located clusters to be aggregated locally to dramatically reduce communication overhead.

Figure 7 shows the workload distribution and memory usage of the SIFT1B dataset optimized using our data placement approach. For detailed setting, please refer to Section 5. The results show that, with the above optimizations, we are able to achieve a balanced workload across DPUs and the memory size used on each DPU does not vary significantly.

Online Query Scheduling. At online phase, the cluster filtering stage selects $nprobe$ clusters for each query. This stage only compares the centroid vectors with the query vectors for filtering, thus is relatively light-weighted compared to the other three stages. We execute this stage and the query scheduling algorithm on the host CPU and send the scheduling results to PIM for actual searching.

Since some popular clusters are replicated and distributed across DPUs, the query scheduling algorithm selects the appropriate replica of the cluster for a query to ensure workload balance. This can be considered as a *load balancing bin-packing problem with constraints* on which bins each item can fit into. We design a greedy algorithm to solve the problem as shown in Algorithm 2. Specifically, we first schedule the clusters with only one replica (Line 4-5). Next, we update the workload on each DPU (Line 6) and continue to schedule the clusters with more than one replicas (Line 8-14). We order these clusters in descending order according to cluster sizes, and iteratively select the DPU with the least workload for each cluster. The algorithm returns a vector named *Assigned*, where the i -th element contains the list of $\langle q_id, c_id \rangle$ pairs scheduled to execute on DPU i . According to *Assigned*, we send the corresponding $q - c$ vectors to the DPUs for execution. Algorithm 2 runs at online phase, with a complexity of $O(|Q| \times nprobe)$. Both $|Q|$ and $nprobe$ are very small compared to the billion-scale data sizes, making the overhead of this algorithm negligible.

4.2 PIM Resource Management

In the last subsection, the PIM-aware workload distribution has promised balanced workloads across DPUs. In this subsection, we discuss how to efficiently manage the limited

Algorithm 2 Query Scheduling for a batch Q

Input: s_i : #vectors in cluster i ; C : centroid vectors;
 M : the cluster to DPU mapping generated by Algorithm 1;
Output: *Assigned*: the query scheduling result;

```

1:  $W[i] \leftarrow 0$  for  $i \in \{0, \dots, ndpu - 1\}$ ;  $\triangleright W[i]$  denotes the workload on DPU  $i$ 
2: for  $i \in [0, |Q| - 1]$  do
3:    $F[i] \leftarrow \text{cluster\_filtering}(Q[i]);$   $\triangleright$  IDs of selected clusters for query  $i$ 
4:   for each cluster  $j$  in  $F[i]$  and  $M[j].size = 1$  do  $\triangleright$  clusters with one replica
5:      $Assigned[M[j][0]].push(\langle i, j \rangle);$   $\triangleright$  Schedule cluster  $j$  of query  $i$  to
       DPU  $M[j][0]$ 
6:      $W[M[j][0]] \leftarrow W[M[j][0]] + s_j;$ 
7:     Remove cluster  $j$  from  $F[i]$ ;
8: Sort all clusters in  $F$  in descending order according to their sizes;
9: for each cluster  $c$  in  $F$  do
10:   $dpus \leftarrow M[c];$   $\triangleright$  the list of DPUs containing replicas of cluster  $c$ 
11:  for each query  $Q[i]$  and  $F[i]$  contains  $c$  do
12:    find  $j$  with  $\min(W[dpus[j]] + s_c);$   $\triangleright$  find the least loaded DPU
13:     $Assigned[dpus[j]].push(\langle i, c \rangle);$ 
14:     $W[dpus[j]] \leftarrow W[dpus[j]] + s_c;$ 

```

resources within each DPU to improve system performance. Specifically, we optimize the thread scheduling and memory management on PIM to better meet application needs.

Thread Scheduling. The UPMEM architecture provides a parallel structure between DPUs, and each DPU is equipped with up to 24 hardware threads and a 14-stage pipeline, effectively mitigating the impact of memory access latency. To efficiently utilize the multi-threads, we can explore hardware parallelism at various levels: between queries, among different clusters of a single query, or within a cluster.

Note that multiple threads operating on the same DPU share the limited resources of 64KB WRAM. Since accessing data from WRAM is much faster than from MRAM, we try to fit all data needed during thread execution in WRAM, including the codebook, LUT and encoded data in selected clusters. The codebook size can be estimated as $D \times 256$, where D represents the dimension of data points, amounting to 32KB for the SIFT dataset. The LUT size can be estimated as $M \times 256 \times \text{sizeof}(\text{uint16})$, which is 8KB when the dimension of encoded points M is 16. If we pursue parallelism at the query or cluster level, the WRAM space will be over-utilized since the combined size of the LUTs for more than four clusters will easily exceed 64KB. Given this hardware constraint, we implement multi-threading within each cluster.

Each DPU is assigned with multiple clusters according to the query scheduling results of Algorithm 2. On each DPU, clusters are processed sequentially while multiple threads execute concurrently to accelerate the processing of a single cluster. Figure 8 illustrates our multi-threading strategy. Specifically, multiple threads split the LUT construction workload by concurrently reading the codebook B from MRAM to WRAM to create a segment of the LUT. After the LUT is constructed, the partial sum of high-frequency co-occurrence combinations are computed using the LUT (details introduced in Section 4.3). The partial sums and the LUT will be combined to construct the full LUT. Once the full LUT is constructed, multiple threads concurrently read the encoded points E from MRAM to WRAM to calculate

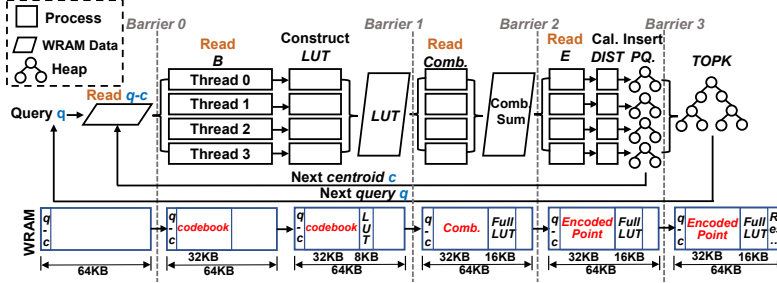


Figure 8. Parallel processing of each cluster inside a single DPU. Red texts represent that the WRAM space is reused.

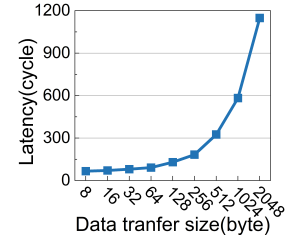


Figure 9. MRAM read latency

the partial distances between the query and search points. Pipelining is enabled to overlap MRAM reads and distance calculations to hide the high latency. Each thread maintains a thread-local priority queue (PQ), implemented as a max heap with a size of k , to store the local top- k partial distances. After a thread finishes the partial top- k insertion, it moves on to process the next cluster.

Four *barriers* are introduced to synchronize the threads and guarantee the correctness of processing. *Barrier 0* prevents premature LUT updates while some threads are still calculating DIST based on LUT. *Barrier 1* ensures the LUT is fully constructed before combination sums are created. *Barrier 2* secures the updated LUT and combination sums, preventing erroneous reads. *Barrier 3* confirms that all threads have completed the distance calculations and result insertions for the current query, allowing for aggregating the final top- k from the thread-local priority queues.

The number of threads (#threads) is an important parameter in the implementation. A DPU can support up to 24 threads. However, since the size of the MRAM-WRAM transfer must be a multiple of 8, at least equal to 8 and not greater than 2048, each thread requires up to 2KB WRAM space to store the search points read from MRAM. Next, we discuss how to efficiently reuse the limited WRAM capacity to allow more threads for better performance.

Memory Management. Due to the significant bandwidth difference between WRAM and MRAM, we aim to maximize the data stored in WRAM. The UPMEM DPU lacks a Memory Management Unit (MMU) to virtualize its physical memory, and the DPU is constrained to the limited physical memory capacity. Therefore, we propose a WRAM reuse strategy specifically tailored to the query processing stages on PIM. This strategy enables multiple threads to operate in a larger address space than the physical WRAM space available.

Figure 8 illustrates the reuse strategy using the SIFT dataset as an example. During the LUT construction stage, we use multiple threads to read the codebooks (32KB) and compute the corresponding entries in the LUT (8KB). Once the complete LUT is obtained, we use the same capacity to construct the sum of the combinations (8KB). Since the codebooks will not be used in the following phases, they can be safely

overwritten to conserve space. As a result, the total space required for the codebooks and the full LUT is only 48KB. Once the full LUT is obtained, we proceed to the distance calculation stage, which is the most time-consuming stage due to the costly encoded point fetching from MRAM to WRAM. To optimize this process, we reuse the WRAM space occupied by codebooks to allow more threads to load encoded data points concurrently. In the example shown in Figure 8, we utilize 16 threads consuming 32KB of memory.

The read latency of MRAM does not increase linearly with size, as shown in Figure 9. The MRAM read latency increases slowly as the data size grows from 8B to 256B. Beyond 256B, the latency rises nearly linearly. This suggests that smaller MRAM read sizes (under 256B) yield greater benefits. Larger MRAM reads can consume significant WRAM space with minimal returns. We explore an optimal MRAM read size (buffer size) to enhance overall efficiency.

4.3 Co-occurrence Aware Encoding

The limited computation and storage resources on a single DPU motivate us to prune the workload needed on DPUs to further improve ANNS efficiency. Existing work have proposed various workload pruning techniques using distance bound [7, 17] and machine learning [44]. These methods can be useful to MemANNS, but are still not good enough.

We observe that items in the encoded points are indices pointing to the codebooks, thus resulting in limited values that typically range from 0 to 255. This allows for certain item combinations to co-occur. Figure 10 shows the maximum co-occurrence frequency of item combinations with lengths 3, 4 and 5 in the SIFT1B dataset. For example, when the length is 3, there could be 256^3 possible item combinations. We count the occurrences of each combination in the encoded points and Figure 10 shows the maximum counts at different lengths. Notably, shorter combinations tend to have a higher frequency of co-occurrence. For example, the most frequently co-occurring combination of length 3 was found in 5.7% of all encoded points. By caching the partial sums of these high-frequency combinations at offline, we can reduce the memory accesses and computations required during the distance calculation stage at runtime, hence greatly alleviating the performance bottleneck.

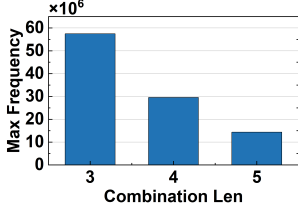


Figure 10. Max. freq. of comb. with different lengths

Avg. Length Reduction	Time Reduction
0	0
0.25	18%
0.5	36%
0.75	54%

Table 1. Higher code length reduction leads to higher query search time reduction

Utilizing the above observation, we propose a *co-occurrence aware data encoding*. Specifically, we adopt a graph-based approach [49] which builds an Item Co-occurrence Graph (ICG) to track item co-occurrences and apply a clustering algorithm to identify frequently accessed combinations of varying lengths. For each cluster, we use this algorithm [49] to select m most frequent combinations of length 3. Combinations with longer lengths can be selected if given larger cache size (WRAM size). The parameter m is also decided by WRAM size and by default, we set it to 256. Our goal is to cache the partial sum of these combinations to avoid repeated computations during online search. However, the distances are unknown at offline phase and the partial sum cannot be pre-computed. Instead, we propose to reserve a buffer space in WRAM to store the partial sum obtained after the LUT construction stage. We pre-arrange the buffer space and generate the memory address for each partial sum. The cache address will be used to re-encode the IVFPQ encoded points. Figure 11 gives a detailed example.

First, as shown on the top of the figure, we use ICG to identify three co-occurrence item sets, namely (1, 15, 26), (79, 25, 77) and (2, 14, 31). Note that, different from existing work [49] which only considered the occurrence of certain items, we must also take into account the positions where these occurrences happen. For example, when utilizing the cached partial sum of the combination (1, 15, 26), it is crucial that these items appear in the columns (0, 1, 2) respectively to make the sum meaningful. **Second**, we calculate the cache address for the partial sum of all possible combinations in the co-occurrence sets. **Third**, we use the generated cache address to re-encode an encoded vector, which has 16 dimensions and each dimension is a *uint8* value in the 0-255 range. This vector contains the high-frequency combinations (1, 15, 26), (79, 25, 77) and (14, 31) on the correct positions. According to the pre-computed cache address, we can find the partial sum of the three combinations at 0x00111, 0x01111 and 0x10110 respectively. Thus, in the new encoded vector, we use the address of the partial sum to replace the original items in the vector. Specifically, the new encoded vector contains three parts. The first digit represents the total length of the vector, followed by the original code which are not identified as high-frequency co-occurred items. These codes are stored as *uint16* to include the column index information.

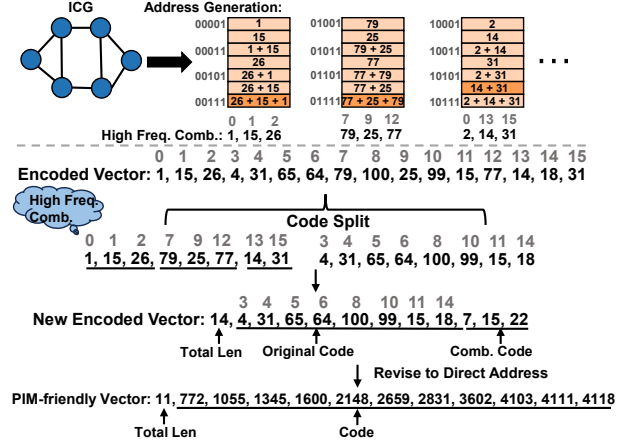


Figure 11. An example of co-occurrence aware encoding.

The combination codes are appended in the end, represented using *uint16* cache addresses of partial sums. The entire process described above is executed during the offline phase.

During online phase, we calculate the partial sums using constructed LUT and store the sums in WRAM according to pre-arranged layout. For example, for combination (1, 15, 26) on position (0, 1, 2), the partial sum is calculated as $LUT[1 + 0 \times 256] + LUT[15 + 1 \times 256] + LUT[26 + 2 \times 256]$, and stored at address 0x00111. By reusing the cached partial sum, we can greatly reduce the computation and memory accesses needed during distance calculation stage.

Note that, during partial sum calculation, we need multiplication operations to access the LUT (e.g., $15 + 1 \times 256$). However, existing work [22] shows that multiplication operations on PIM are less efficient. To mitigate this issue, as shown in Figure 11, we further modify the new encoded vector by converting the original code and combination code into *direct addresses*. The direct address of the original code can be calculated using the code and its column index. We store partial sums in a contiguous memory space after LUT. Thus, the direct address of a combination code can be calculated using the total size of LUT and the code. For example, for combination code 7, it is converted to $16 \times 256 + 7 = 4103$.

In the example, our co-occurrence aware encoding reduces the length of the encoded vector from 16 to 12, achieving a 25% reduction in length. Our empirical studies indicate that, a higher length reduction rate corresponds to a greater decrease in distance calculation time, as demonstrated in Table 1. In our evaluations, we implement this new encoding strategy only when the average length reduction exceeds 50% to avoid negatively affecting the compression rate.

4.4 Top-K Pruning

The above optimizations try to alleviate the memory bottleneck in the LUT construction and distance calculation stages. In this subsection, we look at the performance issue in the top-k selection stage to further enhance MemANNS efficiency.

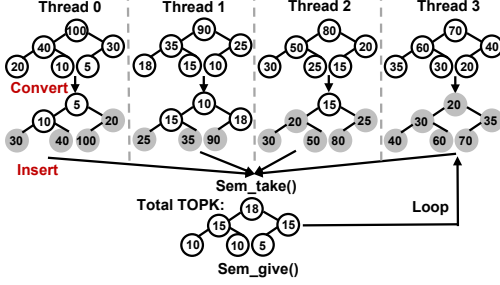


Figure 12. Top-K pruning in DPU. Grey nodes are pruned.

Recall from Figure 8, each thread maintains a thread-local priority queue for local top-k. We get the total top-k on the current DPU by aggregating the local top-k results from different threads. Directly transferring all local top-k to the CPU would lead to too much communication between the CPU and DPUs. Instead, we propose to efficiently insert the values from the local top-k queues into the total top-k queue on the current DPU, with pruning enabled. Figure 12 shows a detailed example.

Considered four threads, each maintaining a priority queue of six items. A max heap is employed to construct the priority queues. Once all four threads have completed their maintenance of the max heaps (Barrier 3), they can use semaphores to concurrently insert values from their thread-local heaps into the total top-k. To minimize unnecessary insertion, we propose to convert the thread-local max heaps into min heaps. We use the `sem_take()` and `sem_give()` semaphore functions to manage concurrent insertions of the top element from each min heap into the total result max heap. For any thread-local min heap, if the top value is greater than the maximum value in the total max heap, it indicates that the remaining values in the thread-local heap cannot contribute to the overall top-k and can therefore be pruned.

5 Evaluation

5.1 Experimental Setup

Compared Baselines. We compare PIM-based MemANNS with CPU-based and GPU-based IVFPQ methods implemented using Faiss [15], a popular ANNS library developed by Meta. There are other advanced works to accelerate ANNS methods. FANNS [28] employs FPGA to accelerate the IVFPQ method but is limited by its device memory, making it unsuitable for billion-scale searches. ANNA [34] designs specialized architecture to accelerate the IVFPQ method based on a simulator. Since MemANNS is based on real-world hardware, ANNA is not a suitable comparison. Juno [38] uses RT cores in GPUs to accelerate the IVFPQ method, but it achieves similar performance to Faiss on GPUs without RT cores, such as A100.

Hardware Setup. Table 2 shows the hardware specifications of the three compared solutions. For the CPU-based platform, we use two Intel Xeon Silver 4110@2.10GHz CPUs

with 4 DDR4-2666Hz DRAM modules, providing 128 GB memory capacity and 85.3 GB/s bandwidth. We use one NVIDIA A100 GPU [41] with 80GB memory capacity and 1,935 GB/s bandwidth. For MemANNS, we use 7 UPMEME PIM modules, with 56 GB total memory capacity and 612.5 GB/s aggregated bandwidth. Existing study [16] indicates that the peak power of each PIM DIMM is 23.22W, leading to 162W total peak power.

Benchmark. We evaluate the compared baselines using two billion-scale datasets, namely the SIFT1B [27] and SPACEV1B [1]. The SIFT1B dataset is composed of 1 billion 128-dimensional vectors encoded into 16 dimensions. The SPACEV1B dataset contains 1 billion 100-dimensional vectors encoded into 20 dimensions. Both datasets contain 10,000 query vectors and corresponding ground truths for recall calculation. We process 1,000 queries at a time. The optimizations in MemANNS do not impact the recall.

Evaluation Metrics. We compare different solutions mainly based on Query per second (QPS). For GPU-based Faiss, we also compare the QPS per Watt (QPS/W) to evaluate the cost-effectiveness of different solutions.

5.2 Overall Performance Results

We first compare the performance and efficiency of the three compared solutions. Results are shown in Figure 13. The term IVF4096 indicates that 1 billion points are partitioned into 4096 clusters. We vary *nprobe* from 64, 128 to 256, which indicates the number of clusters selected for each query search. All results are normalized to the values obtained from Faiss-CPU or Faiss-GPU when *nprobe* is set to 256 for each individual IVF.

Compared to Faiss-CPU, MemANNS consistently achieves the highest queries per second (QPS) across all settings. Specifically, MemANNS accelerates query search times by 2.3x-4.3x for SIFT1B and by 2.1x-4.0x for SPACEV1B when compared to Faiss-CPU. Notably, under the same IVF setting, both MemANNS and Faiss-CPU experience a decrease in QPS as the *nprobe* increases, due to the increased search workload. Under the same *nprobe*, MemANNS obtains a higher QPS improvement compared to Faiss-CPU when the IVF increases. The reason is that a higher number of clusters results in smaller cluster sizes, which leads to fewer encoded points to search within each cluster and reduces data locality. Hence, the CPU, which has multiple cache layers, does not exhibit a linear increase in QPS with increasing IVF. In contrast, the DPU, which has a small-sized WRAM for cache and MRAM for main memory, is less affected by data locality, enabling MemANNS to achieve greater speedup as IVF increases.

Comparing MemANNS with Faiss-GPU, Figure 13b shows the performance results in terms of QPS, and Figure 13c shows the energy efficiency results in terms of QPS per watt. Overall, MemANNS obtains comparable QPS as Faiss-GPU in most cases, except when IVF is 16384 and *nprobe* is 64. We used Nvidia Nsight [4] to look into the results and found

Hardware	Specifications	Approx. Price	Memory capacity	Peak Power	Bandwidth
CPU [24]	2xIntel Xeon Silver 4110@2.10GHz, 4xDDR4 DRAM	1,400USD	128 GB	190W	85.3 GB/s
GPU [41]	Nvidia A100 PCI-e 80GB	20,000USD	80 GB	300W	1935 GB/s
PIM [16]	7xUPMEM PIM (896 DPUs)	2,800USD	56 GB	162W	612.5 GB/s

Table 2. Specifics of evaluated hardware architectures.

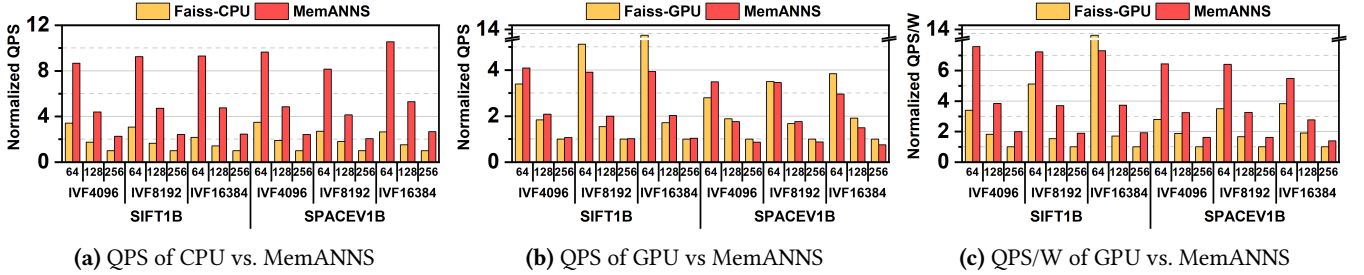


Figure 13. Normalized QPS and QPS/W of different ANNS solutions. *nprobe* varies from 64, 128 to 256. #clusters varies from 4096, 8192 to 16384.

that the significantly high performance of Faiss-GPU under this setting is because of the high parallelism of the top-k selection. The parallelism of this stage on SIFT1B is 9x higher than that on SPACEV1B under the same IVF and *nprobe* parameters. Note that the comparable performance of MemANNS and Faiss-GPU are obtained under a huge gap in the memory bandwidth and computing capabilities between PIM and A100 hardware, as detailed in Table 2.

From the energy efficiency perspective, the 7 UPMEM DIMMs consume 162W peak power while A100 GPU consumes a significant 300W. Although the actual energy consumption during runtime differs from the peak power, we can use it as an approximation to compare the energy efficiency of MemANNS and Faiss-GPU. Results in Figure 13c show that, MemANNS achieves 2x higher QPS/W compared to Faiss-GPU in most cases, demonstrating better power efficiency. Beyond energy consumption, we also find that the per dollar QPS of MemANNS can be up to 9.3x higher than that of Faiss-GPU, indicating that MemANNS can significantly reduce costs in real production environments.

5.3 Scalability Study

Existing systems can hold up to 20 UPMEM DIMMs, each containing 128 DPUs [22], totaling 2560 DPUs. To study the performance of MemANNS beyond the seven PIM DIMMs we have, we evaluate the QPS of MemANNS with 500, 600, ..., 900 DPUs and use the regression method to predict the QPS of MemANNS with up to 2560 DPUs. Due to the limited memory capacity when the number of DPUs is low, we evaluate the performance using the 500 million scale of the SIFT and SPACE datasets.

As shown in Figure 14, the regression curve fits perfectly with the QPS results measured from 500-900 DPUs. When

the number of DPUs increases, the QPS of MemANNS increases almost linearly, demonstrating good scalability of our system. When the number of DPUs is 2560, MemANNS can achieve up to 2.7x higher QPS compared to Faiss-GPU. Note that, even with 20 DIMMs, the cost of PIM is still much lower than that of A100 GPU (\$8000 vs. \$20,000). If we compare the performance of MemANNS and Faiss-GPU under the same peak power (i.e., 300W), we can use 1654 DPUs. As shown by the blue vertical dash line in Figure 14, MemANNS obtains higher QPS than Faiss-GPU at the same peak power constraint under all settings. This again demonstrates the energy efficiency of MemANNS, making it a practical solution for real-world large-scale production systems.

5.4 Sensitivity Study

In this subsection, we study the impact of several parameters to the performance of MemANNS, including the data size of each MRAM read, the number of threads during parallel execution in a single DPU and the required *k* size in the top-k query.

5.4.1 MRAM Read Size. As described in Section 4.2, the MRAM read latency does not increase linearly with size. To decide an optimal MRAM read size for each thread, we evaluate the performance of MemANNS with varied MRAM read sizes. Since the MRAM read size must be between 8 Bytes - 2048 Bytes and aligned with 8 Bytes, we varied the number of vectors read at once. For SIFT1B, we vary the number of vectors fetched in one MRAM read from 2, 4, ..., to 64, making the MRAM read size vary from 64 Bytes, 128 Bytes, ..., to 2 KB. For SPACEV1B, since the dimension of each encoded vector is 20, we vary the number of vectors in one MRAM read from 2, 4, ..., to 32 to fit in the 2048 Bytes limit. We set IVF to 4096 and top-k to 10, testing on 14 threads. Figure 15 shows the evaluation results.

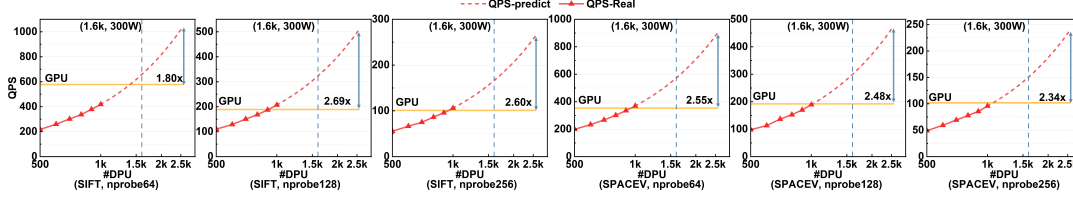


Figure 14. Scalability of MemANNS under different #DPUs. Red triangles are measured from real hardware and red dash line represents predicted QPS. The yellow line indicates the QPS of Faiss-GPU. The blue vertical dash line shows when DPUs consume power equal to that of an A100 GPU.

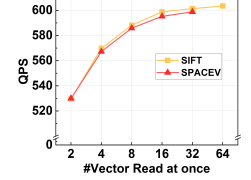


Figure 15. The impact of MRAM read size.

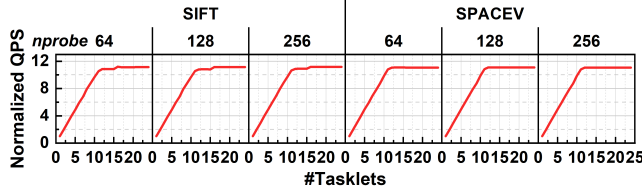
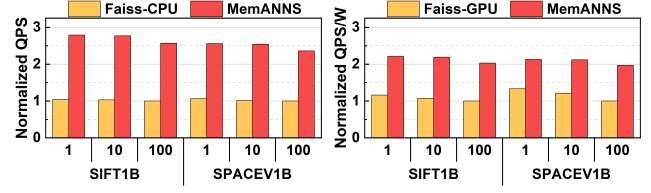


Figure 16. QPS of MemANNS as the #threads increases.



(a) MemANNS vs. CPU

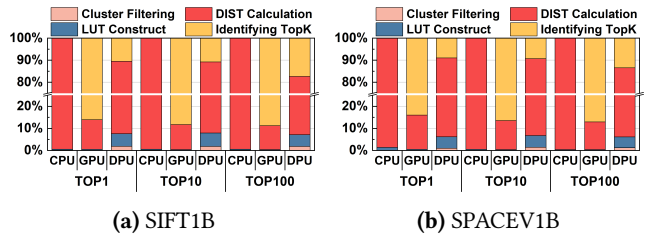
(b) MemANNS vs. GPU

Figure 17. The impact of top-k size

For both datasets, the QPS increases more rapidly when the number of vectors increases from 2 to 16, while becoming much more stable when the number of vectors exceeds 16. This is consistent with our observation in Figure 9, which shows that the MRAM read latency grows slowly when the data transfer size increases from 8 Bytes to 512 Bytes and grows dramatically beyond 512 Bytes. By default, we set the MRAM read size to 16 vectors to have good QPS and reasonable WRAM size at the same time.

5.4.2 Number of Threads per DPU. We evaluate the performance of MemANNS by varying the number of tasklets (namely threads in one DPU) from 1 to 24. Figure 16 shows our results for both datasets with different *nprobe* values. We normalized the values to those when the number of tasklets is one. We have similar observations in all settings. That is, the QPS increases linearly as the number of tasklets increases up to 11. Beyond 11 tasklets, the performance nearly saturates. The QPS of MemANNS with 11 tasklets is almost 11x higher than that with a single tasklet. This is because each DPU has a 14-stage pipeline, and only the last three stages can execute in parallel with the first two stages of the next instruction within the same thread. Using more than 11 tasklets makes full use of the pipeline and keeps the DPU busy. Thus, by default, we set the number of threads to 11 per DPU.

5.4.3 Top-K Size. To study the impact of top-k size, we vary the *k* size from 1, 10 to 100 while keeping other parameters as default. We compare the QPS of MemANNS with that of Faiss-CPU, and the QPS/W of MemANNS with that of Faiss-GPU. Figure 17 shows the results. All results are normalized to the corresponding results of the top-100. We have the following observations.



(a) SIFT1B

(b) SPACEV1B

Figure 18. Query search time breakdown

First, given the same *k* size, MemANNS outperforms Faiss-CPU by 2.6x speedup in QPS on average. In terms of energy efficiency, MemANNS achieves more than 2x better QPS/W compared to Faiss-GPU. Second, under different *k* sizes, the QPS of Faiss-CPU remains almost unchanged while the QPS of MemANNS decreases slightly when *k* varies from 1 to 100. This is mainly due to the increased size of the top-*k* list, which causes higher CPU-DPU communication overhead. Faiss-GPU shares a similar trend in QPS change as MemANNS. This is because selecting top-*k* occupies the largest portion of query search time in Faiss-GPU due to the large amount of CUDA stream synchronization overhead.

We further breakdown the query search time of the compared solutions under different *k* sizes, as shown in Figure 18. We have the following observations. First, comparing different hardware under the same *k* size, MemANNS reduces the ratio of the distance calculation stage from 99.5% on Faiss-CPU to 75.5%, indicating that MemANNS is effectively alleviating the memory bottleneck in the CPU-based implementation. Although the GPU is empowered with a much larger memory bandwidth compared to 7 PIM DIMMs, helping to address memory access issues, it incurs considerable CUDA stream synchronization while identifying top-*k*. This

synchronization has emerged as a new bottleneck, consuming more than 85% of processing time for large-scale datasets. In contrast, DPUs do not share this bottleneck and demonstrate performance comparable to that of the GPUs. Secondly, comparing different k sizes, the time spent on the top- k selection stage increases from 84% to 89% on GPU and from 9% to 17% on DPU. The ratio of this stage on CPU remains unchanged due to the major time taken by distance calculation. This is consistent with our analysis of the impact of top- k sizes discussed above.

5.5 Summary and Discussion

The experimental results underscore the advantages of MemANNS in terms of performance, energy efficiency and scalability. Its ability to outperform Faiss-CPU and maintain competitive performance with Faiss-GPU, coupled with its superior energy and cost efficiency, makes MemANNS a compelling solution for large-scale similarity search applications. However, UPMEM reports a maximum integer processing capacity of 896 GOPS [22], whereas GPUs like A100 offer significantly higher computational power at 156 TFLOPS [41]. In addition, it is essential to mitigate the huge latency gap between multiplication and addition operations in DPU. As UPMEM is the first commercial PIM hardware to enter the market, future versions are expected to enhance computational capacity.

6 Related Work

Existing methods to improve ANNS performance can be categorized into software-based and hardware-based methods.

Software-based Methods. Software-based methods primarily enhance the performance of ANNS through algorithm-level optimizations. For instance, VDTuner [48] utilizes a learning-based parameter tuning method to more quickly find the optimal parameter configuration for ANNS databases. Works such as [7, 17, 35] reduce memory access frequency by establishing a distance or using pruning methods. In contrast, our proposed method accelerates the ANNS algorithm based on new hardware, complementing the aforementioned software-based methods.

Hardware-based Methods. Hardware-based methods primarily accelerate ANNS by utilizing existing hardware or designing new hardware. GPUs are the most commonly used hardware to accelerate ANNS. For example, works such as [21, 31, 52] utilize GPU-based graph methods to accelerate ANNS, but due to the limited and expensive memory capacity in GPUs, it is challenging to scale to large datasets. Juno [38] is based on a compression-based method that uses GPU’s RT-cores to accelerate the IVFPQ method. Compared to graph-based methods, compression-based methods can significantly reduce storage costs, making them better suited to the current situation of rapidly growing data scale. However, compared to MemANNS, these GPU-based methods have a lower energy cost-effectiveness.

In addition to GPUs, many other hardware options have also been used to accelerate ANNS. For example, works such as [5, 28] utilize FPGA to accelerate ANNS. Although this achieves high throughput on million-scale datasets, scaling to billion-scale datasets is limited by the on-chip memory of FPGAs. Conversely, MemANNS is well-suited for billion-scale datasets and offers easy scalability. The works such as [32, 44] utilize SmartSSDs to accelerate ANNS. While this offers a large memory capacity, it has limited bandwidth and can exacerbate the communication bottleneck of PCIe when ANNS is used alongside other applications like recommendation systems and language models (LLMs). In contrast, PIM provides significantly larger and scalable bandwidth, which can communicate with the host via the memory bus without increasing the PCIe communication burden. In addition, the work [25] utilizes *Compute Express Link* (CXL) to accelerate ANNS by incorporating additional memory space and controllers in the main memory. However, this method can significantly increase the cost of system maintenance. In contrast, MemANNS is a cost-effective and easily scalable solution that offers near-linear performance scalability for large-scale datasets.

In addition to existing hardware, many works design new hardware specifically tailored to the characteristics of ANNS for acceleration. For example, [34] proposed a specialized architecture, which combines the benefits of a specialized dataflow pipeline and efficient data reuse to accelerate ANNS. The work [46] proposed a near-data processing (NDP) architecture based on SmartSSD to accelerate the graph-traversal-based ANNS task. However, the aforementioned works are still at the simulation or prototype stage, and are far from practical application.

7 Conclusion

In this work, we addressed the significant performance bottlenecks faced by CPU and GPU-based Approximate Nearest Neighbor Search (ANNS) solutions at billion-scale datasets, where CPU-based solutions are bounded by limited memory bandwidth and GPU-based solutions encounter memory capacity and resource utilization issues. We present MemANNS, a novel framework leveraging UPMEM’s Processing-in-Memory (PIM) architecture to overcome the memory bottleneck in billion-scale ANNS algorithms. MemANNS effectively addresses memory bottlenecks by employing architecture-aware data placement, efficient resource management, and a novel encoding approach for the IVFPQ algorithm. Our evaluation demonstrates that MemANNS significantly improves performance, achieving a remarkable 4.3x increase in QPS compared to CPU-based implementations of Faiss, while also matching the performance of GPU-based Faiss systems. Furthermore, MemANNS shows a commendable 2.3x improvement in QPS per Watt compared to GPU solutions, highlighting its superior cost-effectiveness and potential for large-scale applications such as large model serving.

References

- [1] 2021. SPACEV1B: A billion-Scale vector dataset for text descriptors. <https://github.com/microsoft/SPTAG/tree/main/datasets/SPACEV1B>.
- [2] 2023. Introducing the most advanced Processing In Memory product. <https://www.upmem.com/>.
- [3] 2023. UPMEM User Manual. <https://sdk.upmem.com/2023.1.0/index.html>.
- [4] 2024. NVIDIA Nsight Systems. <https://developer.nvidia.com/nsight-systems>.
- [5] Ameer MS Abdelhadi, Christos-Savvas Bouganis, and George A Constantinides. 2019. Accelerated approximate nearest neighbors search through hierarchical product quantization. In *2019 International Conference on Field-Programmable Technology (ICFPT)*. IEEE, 90–98.
- [6] Alexandr Andoni, Piotr Indyk, Thijs Laarhoven, Ilya Razenshteyn, and Ludwig Schmidt. 2015. Practical and optimal LSH for angular distance. *Advances in neural information processing systems* 28 (2015).
- [7] Fabien André, Anne-Marie Kermarrec, and Nicolas Le Scouarnec. 2016. Cache locality is not enough: High-performance nearest neighbor search with product quantization fast scan. In *42nd International Conference on Very Large Data Bases*, Vol. 9. 12.
- [8] Akhil Arora, Sakshi Sinha, Piyush Kumar, and Arnab Bhattacharya. 2018. Hd-index: Pushing the scalability-accuracy boundary for approximate knn search in high-dimensional spaces. *arXiv preprint arXiv:1804.06829* (2018).
- [9] Arthur Bernhardt, Andreas Koch, and Ilia Petrov. 2023. Pimdb: From main-memory dbms to processing-in-memory dbms-engines on intelligent memories. In *Proceedings of the 19th International Workshop on Data Management on New Hardware*. 44–52.
- [10] Shuangyu Cai, Boyu Tian, Huanchen Zhang, and Mingyu Gao. 2024. PimPam: Efficient Graph Pattern Matching on Real Processing-in-Memory Hardware. *Proceedings of the ACM on Management of Data* 2, 3 (2024), 1–25.
- [11] Faquan Chen, Rendong Ying, Jianwei Xue, Fei Wen, and Peilin Liu. 2023. Parallelnn: A parallel octree-based nearest neighbor search accelerator for 3d point clouds. In *2023 IEEE International Symposium on High-Performance Computer Architecture (HPCA)*. IEEE, 403–414.
- [12] Rihan Chen, Bin Liu, Han Zhu, Yaoxuan Wang, Qi Li, Buting Ma, Qingbo Hua, Jun Jiang, Yunlong Xu, Hongbo Deng, et al. 2022. Approximate nearest neighbor search under neural similarity metric for large-scale recommendation. In *Proceedings of the 31st ACM International Conference on Information & Knowledge Management*. 3013–3022.
- [13] Sitian Chen, Haobin Tan, Amelie Chi Zhou, Yusen Li, and Pavan Balaji. 2024. UpDLRM: Accelerating Personalized Recommendation using Real-World PIM Architecture. *Proceedings of the 56th Annual Design Automation Conference (DAC)* (2024).
- [14] Fabrice Devaux. 2019. The true processing in memory accelerator. In *HCS'19*. IEEE Computer Society, 1–24.
- [15] Facebook AI Research. [n.d.]. Faiss. <https://github.com/facebookresearch/faiss>.
- [16] Yann Falevoz and Julien Legriel. 2023. Energy efficiency impact of processing in memory: A comprehensive review of workloads on the upmem architecture. In *European Conference on Parallel Processing*. Springer, 155–166.
- [17] Jianyang Gao and Cheng Long. 2023. High-dimensional approximate nearest neighbor search: with reliable and efficient distance comparison operations. *Proceedings of the ACM on Management of Data* 1, 2 (2023), 1–27.
- [18] Christina Giannoula, Peiming Yang, Ivan Fernandez Vega, Jiacheng Yang, Yu Xin Li, Juan Gomez Luna, Mohammad Sadrosadati, Onur Mutlu, and Gennady Pekhimenko. 2024. Accelerating Graph Neural Networks on Real Processing-In-Memory Systems. *arXiv:2402.16731 [cs.AR]* <https://arxiv.org/abs/2402.16731>
- [19] Kailash Gogineni, Sai Santosh Dayapule, Juan Gómez-Luna, Karthikeya Gogineni, Peng Wei, Tian Lan, Mohammad Sadrosadati, Onur Mutlu, and Guru Venkataramani. 2024. SwiftRL: Towards Efficient Reinforcement Learning on Real Processing-In-Memory Systems. *arXiv preprint arXiv:2405.03967* (2024).
- [20] Long Gong, Huayi Wang, Mitsunori Ogihara, and Jun Xu. 2020. iDEC: indexable distance estimating codes for approximate nearest neighbor search. *Proceedings of the VLDB Endowment* 13, 9 (2020).
- [21] Fabian Groh, Lukas Ruppert, Patrick Wieschollek, and Hendrik PA Lensch. 2022. Ggnn: Graph-based gpu nearest neighbor search. *IEEE Transactions on Big Data* 9, 1 (2022), 267–279.
- [22] Juan Gómez-Luna, Izzat El Hajj, Ivan Fernandez, Christina Giannoula, Geraldo F. Oliveira, and Onur Mutlu. 2022. Benchmarking a New Paradigm: Experimental Analysis and Characterization of a Real Processing-in-Memory System. *IEEE Access* 10 (2022), 52565–52608.
- [23] Bongjoon Hyun, Taehun Kim, Dongjae Lee, and Minsoo Rhu. 2024. Pathfinding Future PIM Architectures by Demystifying a Commercial PIM Technology. In *2024 IEEE International Symposium on High-Performance Computer Architecture (HPCA)*. IEEE, 263–279.
- [24] Intel. 2017. Intel Xeon Silver 4110 Processor. <https://www.intel.com/content/www/us/en/products/sku/123547/intel-xeon-silver-4110-processor-11m-cache-2-10-ghz/specifications.html>.
- [25] Junhyeok Jang, Hanjin Choi, Hanyeoreum Bae, Seungjun Lee, Miryeong Kwon, and Myoungsoo Jung. 2023. CXL-ANNS: Software-Hardware Collaborative Memory Disaggregation and Computation for Billion-Scale Approximate Nearest Neighbor Search. In *2023 USENIX Annual Technical Conference (USENIX ATC 23)*. Boston, MA, 585–600.
- [26] Herve Jegou, Matthijs Douze, and Cordelia Schmid. 2010. Product quantization for nearest neighbor search. *IEEE transactions on pattern analysis and machine intelligence* 33, 1 (2010), 117–128.
- [27] Hervé Jégou, Romain Tavenard, Matthijs Douze, and Laurent Amsaleg. 2011. Searching in one billion vectors: re-rank with source coding. In *2011 IEEE International Conference on Acoustics, Speech and Signal Processing (ICASSP)*. IEEE, 861–864.
- [28] Wenqi Jiang, Shigang Li, Yu Zhu, Johannes De Fine Licht, Zhenhao He, Runbin Shi, Cedric Renggli, Shuai Zhang, Theodoros Rekatsinas, Torsten Hoefer, and Gustavo Alonso. 2023. Co-design Hardware and Algorithm for Vector Search. In *Proceedings of the International Conference for High Performance Computing, Networking, Storage and Analysis (SC '23)*. Article 87, 15 pages.
- [29] Muhammad Attahir Jibril, Hani Al-Sayeh, and Kai-Uwe Sattler. 2024. Accelerating Aggregation Using a Real Processing-in-Memory System. In *2024 IEEE 40th International Conference on Data Engineering (ICDE)*. Los Alamitos, CA, USA, 3920–3932.
- [30] Jeff Johnson, Matthijs Douze, and Hervé Jégou. 2019. Billion-scale similarity search with GPUs. *IEEE Transactions on Big Data* 7, 3 (2019), 535–547.
- [31] Saim Khan, Somesh Singh, Harsha Vardhan Simhadri, Jyothi Vedurada, et al. 2024. BANG: Billion-Scale Approximate Nearest Neighbor Search using a Single GPU. *arXiv preprint arXiv:2401.11324* (2024).
- [32] Ji-Hoon Kim, Yeo-Reum Park, Jaeyoung Do, Soo-Young Ji, and Joo-Young Kim. 2023. Accelerating Large-Scale Graph-Based Nearest Neighbor Search on a Computational Storage Platform. *IEEE Trans. Comput.* 72, 1 (2023), 278–290.
- [33] Pau Perng-Hwa Kung, Zihao Fan, Tong Zhao, Yozen Liu, Zhixin Lai, Jiahui Shi, Yan Wu, Jun Yu, Neil Shah, and Ganesh Venkataraman. 2024. Improving Embedding-Based Retrieval in Friend Recommendation with ANN Query Expansion. In *Proceedings of the 47th International ACM SIGIR Conference on Research and Development in Information Retrieval*. 2930–2934.
- [34] Yejin Lee, Hyunji Choi, Sunhong Min, Hyunseung Lee, Sangwon Beak, Dawoon Jeong, Jae W Lee, and Tae Jun Ham. 2022. Anna: Specialized architecture for approximate nearest neighbor search. In *2022 IEEE*

International Symposium on High-Performance Computer Architecture (HPCA). IEEE, 169–183.

- [35] Daniel LeJeune, Reinhard Heckel, and Richard Baraniuk. 2019. Adaptive estimation for approximate k -nearest-neighbor computations. In *The 22nd International Conference on Artificial Intelligence and Statistics*. PMLR, 3099–3107.
- [36] Shiyu Li, Yitu Wang, Edward Hanson, Andrew Chang, Yang Seok Ki, Hai Helen Li, and Yiran Chen. 2024. NDRec: A Near-Data Processing System for Training Large-Scale Recommendation Models. *IEEE Trans. Comput.* (2024).
- [37] Shengwen Liang, Ziming Yuan, Ying Wang, Dawen Xu, Huawei Li, and Xiaowei Li. 2024. HyQA: Hybrid Near-Data Processing Platform for Embedding Based Question Answering System. In *2024 Design, Automation & Test in Europe Conference & Exhibition (DATE)*. IEEE, 1–6.
- [38] Zihan Liu, Wentao Ni, Jingwen Leng, Yu Feng, Cong Guo, Quan Chen, Chao Li, Minyi Guo, and Yuhao Zhu. 2024. JUNO: Optimizing High-Dimensional Approximate Nearest Neighbour Search with Sparsity-Aware Algorithm and Ray-Tracing Core Mapping. In *Proceedings of the 29th ACM International Conference on Architectural Support for Programming Languages and Operating Systems, Volume 2* (<conf-loc>, <city>La Jolla</city>, <state>CA</state>, <country>USA</country>, </conf-loc>) (*ASPLOS '24*). 549–565.
- [39] Yu A Malkov and Dmitry A Yashunin. 2018. Efficient and robust approximate nearest neighbor search using hierarchical navigable small world graphs. *IEEE transactions on pattern analysis and machine intelligence* 42, 4 (2018), 824–836.
- [40] Magdalen Dobson Manohar, Zheqi Shen, Guy E. Blelloch, Laxman Dhulipala, Yan Gu, Harsha Vardhan Simhadri, and Yihan Sun. 2024. ParlayANN: Scalable and Deterministic Parallel Graph-Based Approximate Nearest Neighbor Search Algorithms. In *Proceedings of the 29th ACM SIGPLAN Annual Symposium on Principles and Practice of Parallel Programming, PPOPP 2024, Edinburgh, United Kingdom, March 2-6, 2024*, Michel Steuwer, I-Ting Angelina Lee, and Milind Chabbi (Eds.). ACM, 270–285.
- [41] Nvidia. 2020. NVIDIA A100. <https://www.nvidia.cn/data-center/a100/>.
- [42] Steve Rhyner, Haocong Luo, Juan Gómez-Luna, Mohammad Sadrosadati, Jiawei Jiang, Ataberk Olgun, Harshita Gupta, Ce Zhang, and Onur Mutlu. 2024. PIM-Opt: Demystifying Distributed Optimization Algorithms on a Real-World Processing-In-Memory System. In *Proceedings of the 2024 International Conference on Parallel Architectures and Compilation Techniques* (Long Beach, CA, USA) (*PACT '24*). 201–218.
- [43] Yukihiro Tagami. 2017. Annexml: Approximate nearest neighbor search for extreme multi-label classification. In *Proceedings of the 23rd ACM SIGKDD international conference on knowledge discovery and data mining*. 455–464.
- [44] Bing Tian, Haikun Liu, Zhuohui Duan, Xiaofei Liao, Hai Jin, and Yu Zhang. 2024. Scalable Billion-point Approximate Nearest Neighbor Search Using SmartSSDs. In *2024 USENIX Annual Technical Conference (USENIX ATC 24)*.
- [45] Yitu Wang, Shiyu Li, Qilin Zheng, Andrew Chang, Hai Li, and Yiran Chen. 2023. EMS-i: An Efficient Memory System Design with Specialized Caching Mechanism for Recommendation Inference. *ACM Transactions on Embedded Computing Systems* 22, 5s (2023), 1–22.
- [46] Yitu Wang, Shiyu Li, Qilin Zheng, Linghao Song, Zongwang Li, Andrew Chang, Hai "Helen" Li, and Yiran Chen. 2024. NDSEARCH: Accelerating Graph-Traversal-Based Approximate Nearest Neighbor Search through Near Data Processing. In *2024 ACM/IEEE 51st Annual International Symposium on Computer Architecture (ISCA)*. 368–381.
- [47] Weihong Xu, Junwei Chen, Po-Kai Hsu, Jaeyoung Kang, Minxuan Zhou, Sumukh Ping, Shimeng Yu, and Tajana Rosing. 2023. Proxima: Near-storage Acceleration for Graph-based Approximate Nearest Neighbor Search in 3D NAND. *arXiv preprint arXiv:2312.04257* (2023).
- [48] T. Yang, W. Hu, W. Peng, Y. Li, J. Li, G. Wang, and X. Liu. 2024. VDTuner: Automated Performance Tuning for Vector Data Management Systems. In *2024 IEEE 40th International Conference on Data Engineering (ICDE)*. 4357–4369.
- [49] Haojie Ye, Sanketh Vedula, Yuhao Chen, Yichen Yang, Alex Bronstein, Ronald Dreslinski, Trevor Mudge, and Nishil Talati. 2023. GRACE: A Scalable Graph-Based Approach to Accelerating Recommendation Model Inference. In *Proceedings of the 28th ACM International Conference on Architectural Support for Programming Languages and Operating Systems, Volume 3*. 282–301.
- [50] Jiaqi Zhai, Lucy Liao, Xing Liu, Yueming Wang, Rui Li, Xuan Cao, Leon Gao, Zhaojie Gong, Fangda Gu, Jiayuan He, Yinghai Lu, and Yu Shi. 2024. Actions Speak Louder than Words: Trillion-Parameter Sequential Transducers for Generative Recommendations. In *Proceedings of the 41st International Conference on Machine Learning (Proceedings of Machine Learning Research, Vol. 235)*, Ruslan Salakhutdinov, Zico Kolter, Katherine Heller, Adrian Weller, Nuria Oliver, Jonathan Scarlett, and Felix Berkenkamp (Eds.). PMLR, 58484–58509.
- [51] Jianjin Zhang, Zheng Liu, Weihao Han, Shitao Xiao, Ruicheng Zheng, Yingxia Shao, Hao Sun, Hanqing Zhu, Premkumar Srinivasan, Weiwei Deng, et al. 2022. Uni-retriever: Towards learning the unified embedding based retriever in bing sponsored search. In *Proceedings of the 28th ACM SIGKDD Conference on Knowledge Discovery and Data Mining*. 4493–4501.
- [52] Weijie Zhao, Shulong Tan, and Ping Li. 2020. Song: Approximate nearest neighbor search on gpu. In *2020 IEEE 36th International Conference on Data Engineering (ICDE)*. IEEE, 1033–1044.
- [53] Bolong Zheng, Zhao Xi, Lianggui Weng, Nguyen Quoc Viet Hung, Hang Liu, and Christian S Jensen. 2020. PM-LSH: A fast and accurate LSH framework for high-dimensional approximate NN search. *Proceedings of the VLDB Endowment* 13, 5 (2020), 643–655.
- [54] Yuxin Zheng, Qi Guo, Anthony KH Tung, and Sai Wu. 2016. LazyLSH: Approximate nearest neighbor search for multiple distance functions with a single index. In *Proceedings of the 2016 International Conference on Management of Data*. 2023–2037.